

Mitigating Concentration Polarization through Acid–Base Interaction Effects for Long-Cycling Lithium Metal Anodes

Junmou Du,[#] Xiangrui Duan,[#] Wenyu Wang, Guocheng Li, Chunhao Li, Yuchen Tan, Mintao Wan, Zhi Wei Seh, Li Wang, and Yongming Sun*



Cite This: *Nano Lett.* 2023, 23, 3369–3376



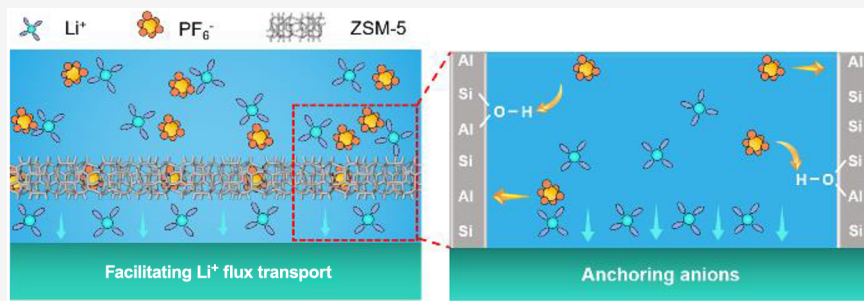
Read Online

ACCESS |

Metrics & More

Article Recommendations

Supporting Information



ABSTRACT: Lithium (Li) metal has attracted great attention as a promising high-capacity anode material for next-generation high-energy-density rechargeable batteries. Nonuniform Li⁺ transport and uneven Li plating/stripping behavior are two key factors that deteriorate the electrochemical performance. In this work, we propose an interphase acid–base interaction effect that could regulate Li plating/stripping behavior and stabilize the Li metal anode. ZSM-5, a class of zeolites with ordered nanochannels and abundant acid sites, was employed as a functional interface layer to facilitate Li⁺ transport and mitigate the cell concentration polarization. As a demonstration, a pouch cell with a high-areal-capacity LiNi_{0.95}Co_{0.02}Mn_{0.03}O₂ cathode (3.7 mAh cm⁻²) and a ZSM-5 modified thin lithium anode (50 μm) delivered impressive electrochemical performance, showing 92% capacity retention in 100 cycles (375.7 mAh). This work reveals the effect of acid–base interaction on regulating lithium plating/stripping behaviors, which could be extended to developing other high-performance alkali metal anodes.

KEYWORDS: lithium metal anode, concentration polarization, Li⁺ transference number, acid–base interaction, interface

Lithium-ion batteries (LIBs) are currently the main power sources for portable electronics and electric vehicles.^{1–3} However, their energy density is gradually approaching the theoretical limit, which calls for the development of new battery systems with a higher energy density.^{4–6} Among lithium (Li) chemistries, rechargeable Li metal batteries (LMBs) have received great attention, which employ Li metal anodes with the highest theoretical capacity of 3860 mAh g⁻¹ and the lowest electrochemical potential (−3.04 V vs. SHE).^{4,6–8} However, the practical application of the Li metal anode is hindered by serious challenges, including nonuniform Li⁺ transport and inhomogeneous Li plating/stripping behavior at the electrode interphases, and even hazardous Li dendrite growth.^{9–13} To improve the electrochemical stability of the Li metal anode, various strategies of interface design have been adopted to improve electrochemical Li plating/stripping cycling. Typically, functional components, such as Li-based alloys (Li–Sn,^{14,15} Li–Al,¹⁶ Li–Si,¹⁷ Li–Zn,¹⁸ etc.) with good lithiophilicity, have been constructed on the surface of the Li metal anode. Their lithiophilic property enabled Li plating with low overpotential and uniform structure. Some lithium

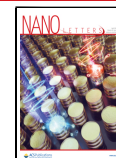
compounds, including LiF,¹⁹ Li₃N,²⁰ Li₃PO₄,²¹ and Li₂S,²² were employed as effective components for Li metal interphase protection, which endowed high interphase ionic conductivity and stability, and improved the Li metal plating/stripping behavior.

Besides the functional components, the rational structural design of interphases could regulate Li⁺ transport characteristics. It has been revealed that lithium dendrite formation is closely associated with the Li⁺ transport property in the vicinity of the lithium electrode.^{23–25} During the charge/discharge processes, an inevitably large Li⁺ concentration gradient exists at the electrode interface, and the situation becomes even more serious under high current density conditions, which would cause an increase in the overpotential, known as concentration

Received: January 31, 2023

Revised: April 6, 2023

Published: April 13, 2023



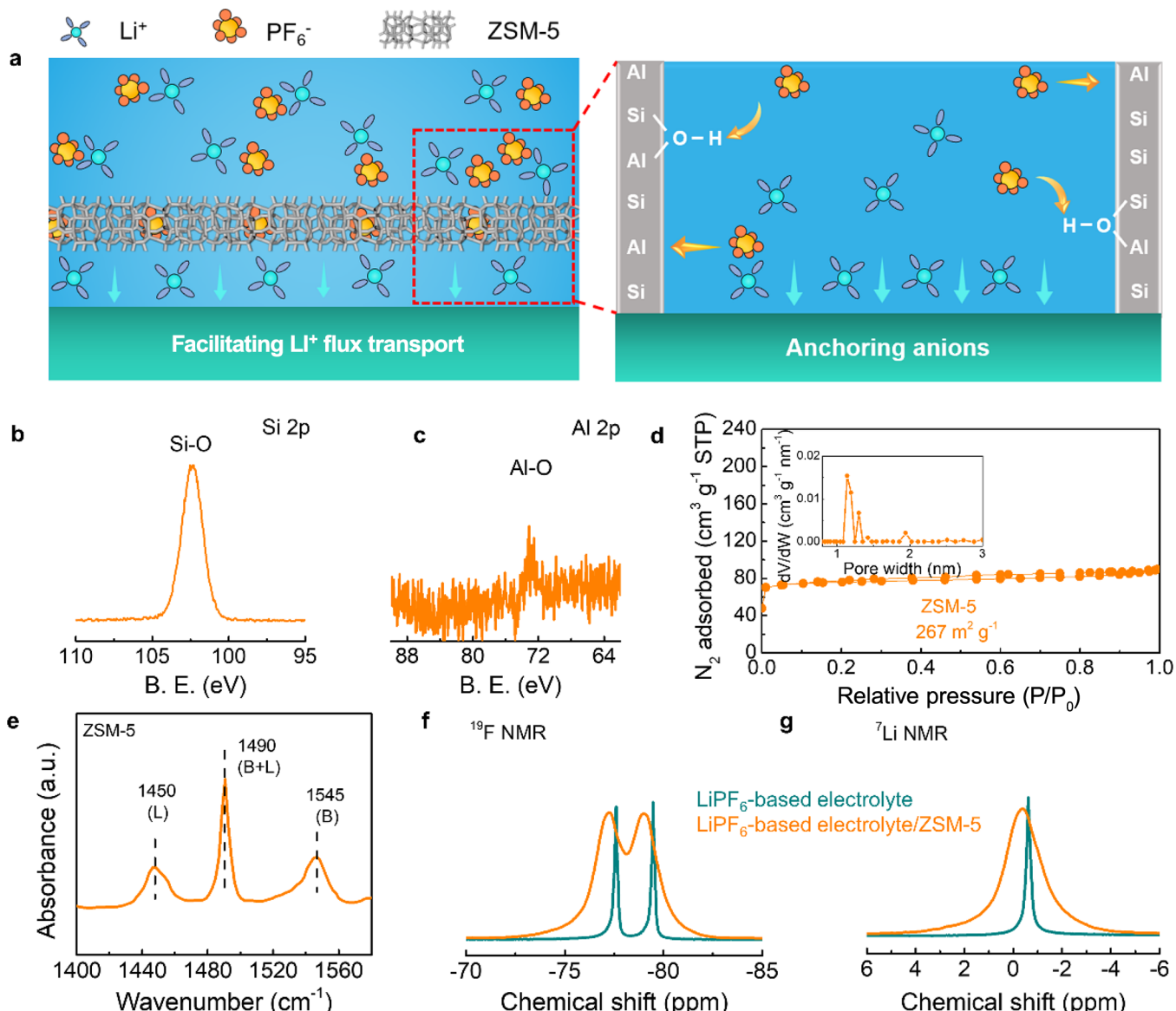


Figure 1. (a) Schematic of the functional ZSM-5 layer for a Li metal anode. PF₆⁻ anions could be anchored on acid sites of ZSM-5 via acid–base interaction, enabling improved Li⁺ transport property. (b) TEM image of ZSM-5. (c) High-resolution Si 2p and Al 2p XPS spectra of ZSM-5. (d) N₂ adsorption/desorption isotherms of a ZSM-5 zeolite (inset is the pore size distribution plot). (e) Py-FTIR analysis of a ZSM-5 zeolite at 200 °C. SSNMR spectra of (f) ¹⁹F and (g) ⁷Li of ZSM-5 filled electrolyte compared with a blank electrolyte.

polarization.^{23,26} According to Sand's time theory, Li⁺ depletion at the electrode interface during Li plating leads to accumulation of electrons and induces the formation of space charge at the electrode interface, and the deficient Li ions tend to plate at the protrusions, leading to nonuniform Li growth and even dendritic lithium deposits.²⁷ Such behavior deteriorates Li electrochemical cycling, and even causes safety hazards. Ideally, accelerating Li⁺ transport while inhibiting the transport of anions can effectively suppress the concentration polarization. Construction of ion-conductive interphase layers on the Li metal anode can help to selectively increase the Li⁺ transference number (t_{Li^+}) and thus buffer concentration polarization. Recently, metal–organic-frameworks (MOFs)²⁸ and covalent–organic-frameworks (COFs)²⁹ have been employed as functional interphases for the Li metal electrode and have shown their success in regulating Li⁺ flux and enabling uniform Li plating due to their ordered pore structures and abundant adsorption sites. However, the

chemical stability of such organic frameworks with Li metal anodes should be further verified, and the high cost and complex preparation process can be an obstacle for their implementation in Li metal batteries.^{30,31} Thus, it is desirable to rationally design interphase structures that could regulate Li⁺ flux and reduce concentration polarization of the Li metal electrode, and to reveal their underlying working mechanism.

Herein, we propose that the Li plating/stripping behavior of the Li metal electrode could be regulated by a novel functional interphase that could anchor anions and facilitate Li⁺ transport (Figure S1). Experimentally, a zeolite layer (ZSM-5) was constructed on the Li metal electrode, which possessed abundant nanochannels with a large surface area. The abundant acid sites on the ZSM-5 framework could anchor anions through acid–base interactions, thus selectively allowing fast Li⁺ transport and enabling homogeneous Li plating at the electrode interface (Figure 1a). The “sieving” effect of ZSM-5 improved the Li⁺ transport property at the Li anode surface,

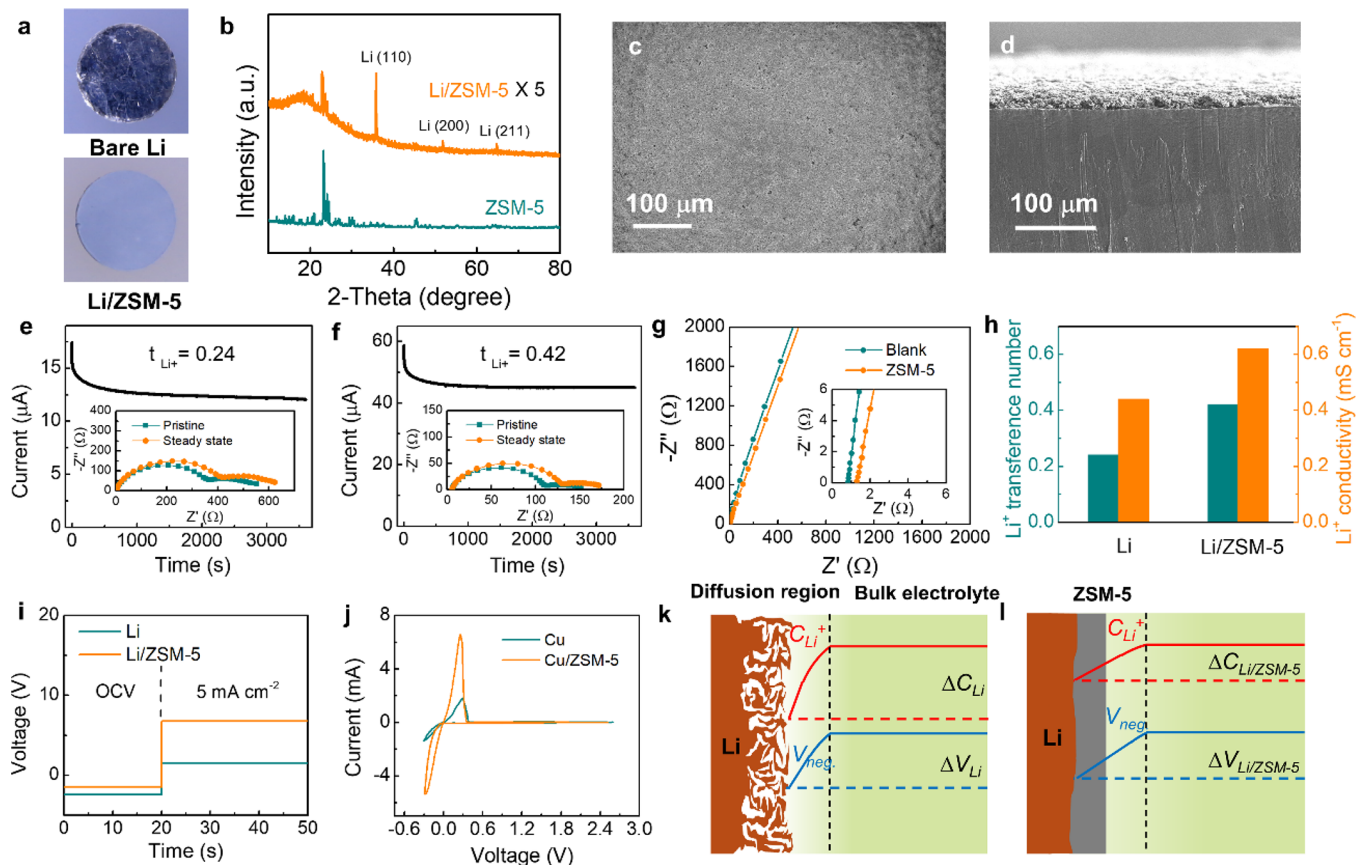


Figure 2. (a) Digital photograph of bare Li and Li/ZSM-5 electrodes. (b) XRD patterns of ZSM-5 and Li/ZSM-5. (c) Top-view and (d) cross-sectional SEM images of the Li/ZSM-5 electrode. Measurement of the Li^+ transference number of (e) $\text{Li}||\text{Li}$ and (f) $\text{Li/ZSM-5}||\text{Li/ZSM-5}$ cells by the potentiostatic polarization method. Insets of (e,f) were the EIS curves of $\text{Li}||\text{Li}$ and $\text{Li/ZSM-5}||\text{Li/ZSM-5}$ cells before and after polarization. (g) Nyquist plots of the EIS test of the bare separator and ZSM-5 coated separator (inset: enlarged EIS curves). (h) The Li^+ transference number and Li^+ conductivity of liquid electrolyte using bare Li and Li/ZSM-5 as electrodes, respectively. (i) Comparison of the voltage response to a current of 5 mA of the bare Li and Li/ZSM-5 electrode sandwiched between two stainless current collectors. (j) CV curve of $\text{Cu}||\text{Li}$ and Cu/ZSM-5 cells. Schematic of the Li^+ concentration gradient at (k) bare Li and (l) Li/ZSM-5 electrode interfaces.

which could efficiently compensate for the continuous Li depletion and minimize the concentration polarization. Furthermore, the chemical inertness and strong mechanical strength of ZSM-5 enabled good structural integrity of the electrode interface, and thus long-term cycling stability of the Li metal anode. With such a design, we demonstrated that a full pouch cell with a high-areal-capacity $\text{LiNi}_{0.95}\text{Co}_{0.02}\text{Mn}_{0.03}$ cathode (3.9 mAh cm^{-2}) and thin Li metal anode ($50 \mu\text{m}$) exhibited superior electrochemical performance with 90% capacity retention for 100 cycles.

Zeolites are known as a class of crystalline silicoaluminates, which are widely used for petroleum refining (Figure S2).³² Figure 1b,c shows the high-resolution Si 2p and Al 2p X-ray photoelectron spectroscopy (XPS) spectra for ZSM-5. The binding energy located at 102.4 and 72.8 eV could be attributed to Si–O and Al–O bonds of the silicoaluminate structure of ZSM-5. The results of the adsorption/desorption curve (Figure 1d) and the pore size distribution plot (inset in Figure 1d) indicate the microporous structure of ZSM-5 and its reasonably high specific surface area of $267 \text{ m}^2 \text{ g}^{-1}$. With abundant nanopores and channels with a size of 0.54 nm ,²⁹ ZSM-5 allowed Li^+ with a smaller size (0.15 nm) to pass through and redistribute its flux at the electrode/ZSM-5 film interface, which was beneficial for homogenizing lithium plating/stripping behavior. Moreover, the acid/base sites of

the material could interact with lithium salt in the electrolyte, altering the Li^+ mobility.^{33–35} The acidic properties of ZSM-5 were measured by pyridine adsorption Fourier transform infrared spectroscopy (Py-FTIR). Pyridine can serve as a probe molecule, which can be adsorbed on the acidic sites of ZSM-5, and the pyridine adsorbed by the Brønsted acid site and Lewis acid site can be detected by an infrared spectrum at different wavenumbers (Figure S3).^{36,37} As shown in Figure 1e, three bands were observed at wavenumbers of 1450, 1545, and 1490 cm^{-1} , which could be assigned to pyridine adsorption onto the Brønsted acid site (B), Lewis acid site (L), and a common peak for both Brønsted acid site and Lewis acid site, respectively (Figure S4).³⁸ This result verified the existence of the surface acid sites of the ZSM-5 zeolite. To explore the regulatory roles of acid sites on the ion transport property, the molecular interaction between ZSM-5 zeolite and the electrolyte was investigated by solid state nuclear magnetic resonance (SSNMR) spectroscopy. Figure 1f,g shows the SSNMR signals of ^{19}F and ^{7}Li for LiPF_6 -based electrolytes. For pure LiPF_6 electrolyte, the sharp peaks were derived from the isotropic diffusion of PF_6^- and Li^+ in the electrolyte. With the addition of ZSM-5, the corresponding peaks became broad, verifying the anisotropic feature of LiPF_6 that interacted with ZSM-5. The addition of ZSM-5 markedly shifted ^{19}F downfield from -77.599 ppm and -79.460 ppm to -77.211 ppm and -79.012 ppm .

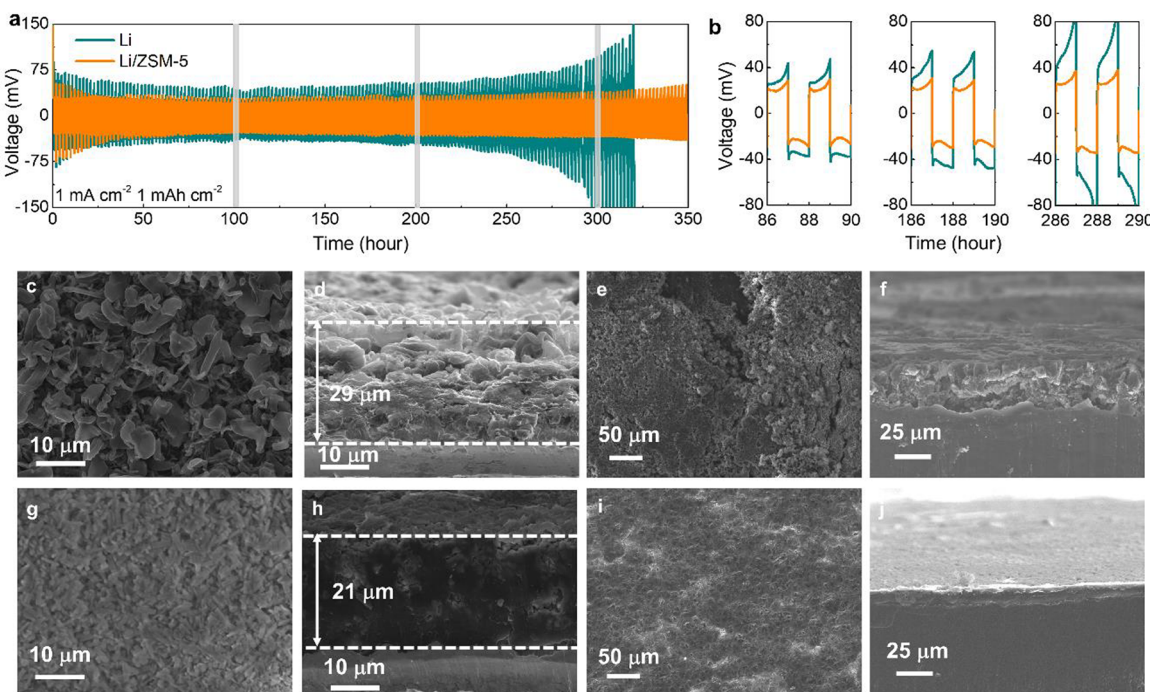


Figure 3. (a, b) Voltage profiles of Li||Li and Li/ZSM-5||Li/ZSM-5 cells at 1 mA cm^{-2} and 1 mAh cm^{-2} . Top-view SEM images of (c) Cu and (g) Cu/ZSM-5 electrodes after initial Li plating at 1 mA cm^{-2} and 4 mAh cm^{-2} , and (d, h) the corresponding cross-sectional SEM images. Top-view SEM images of (e) Li||Li and (i) Li/ZSM-5||Li/ZSM-5 cells after 50 cycles at 1 mA cm^{-2} and 1 mAh cm^{-2} , and (f, j) the corresponding cross-sectional SEM images.

ppm due to the binding effect between PF_6^- anions and the surface acid sites of ZSM-5, and the signal for ^7Li also shifted downfield from -0.644 ppm to -0.334 ppm , supporting weakened ion association of the $\text{Li}^+/\text{PF}_6^-$ pair.³⁹ The obvious chemical shifts indicated the decreasing electron cloud density around both PF_6^- and Li^+ , which can be explained as follows: the acid–base interaction of ZSM-5 with LiPF_6 facilitated the dissociation of LiPF_6 , and the electron-deficient acid sites would interact with anionic PF_6^- , by which the migration of PF_6^- was inhibited. Meanwhile, the PF_6^- anions anchored by acid sites weakened their interaction with Li^+ , which could promote the release of “free” Li^+ . This effect of regulating the chemical environment of Li^+ and PF_6^- in the electrolyte based on the acid–base interaction was beneficial for improving the Li^+ mass transfer and promoting the Li^+ transference number.^{39,40}

A smooth ZSM-5 film was constructed on the Li metal electrode to produce Li/ZSM-5 electrodes as described in the experimental section (Figures S5–S6, Figure 2a). The Li/ZSM-5 electrode showed characteristic powder X-ray diffraction (XRD) peaks for ZSM-5 and metallic lithium without impurities, suggesting the chemical inertness between ZSM-5 and metallic Li (Figure 2b). The top-view SEM image showed that ZSM-5 zeolites were tightly stacked on the surface of the Li metal surface without cracks (Figure 2c and Figure S7) and the cross-sectional SEM and corresponding elemental mapping images revealed a compact ZSM-5 layer on the Li metal surface with a thickness of $\sim 9 \mu\text{m}$ (Figure S8, Figure 2d).

To investigate the enhanced Li^+ mobility of the Li/ZSM-5 electrode, values of t_{Li}^+ of the electrolyte with pristine metallic Li and Li/ZSM-5 electrodes were compared, which were determined by the electrochemical impedance spectroscopy (EIS) corrected response current. As shown in Figure 2e,f, the

value of t_{Li}^+ increased from 0.24 to 0.42 after a combination with the ZSM-5 zeolite (Figure 2h). Such results indicated that the Li^+ electromigration in the Li/ZSM-5 electrode could be accelerated, which was beneficial for mitigating the concentration polarization and inhibiting the formation of Li dendrites. The ionic conductivity of electrolyte was further characterized by EIS (Figure 2g). The ionic conductivity of ZSM-5 coated separator with the electrolyte was calculated to be 1.49 mS cm^{-1} , which was slightly lower than that of the bare electrolyte (1.82 mS cm^{-1}). The decreased ionic conductivity could be attributed to the immobilized PF_6^- anions by ZSM-5. The conductivity of Li^+ was calculated according to the total ionic conductivity and t_{Li}^+ . A higher conductivity of 0.62 mS cm^{-1} was achieved for the ZSM-5 coated separator in comparison to 0.44 mS cm^{-1} for the bare separator (Figure 2h). Therefore, the presence of ZSM-5 in the Li/ZSM-5 electrode could effectively improve the Li^+ transport due to its ordered pore structure and abundant acid sites. The electrical insulation of Li/ZSM-5 was also tested by a direct voltage–current measurement using a stainless steel sandwiched Li metal coin cell. The Li/ZSM-5 electrode showed a 6 times higher voltage response at 5 mA cm^{-2} than the bare Li electrode (7 mV vs. 1 mV), verifying the high electronic resistance of the ZSM-5 interface, which could efficiently block electron leakage and induce Li plating at the bottom of the ZSM-5 layer (Figure 2i).

The electrochemical property of the ZSM-5 layer was evaluated by a cyclic voltammetry (CV) test. As shown in Figure 2j, the much higher current peak of the Cu/ZSM-5 electrode indicated a higher Li^+ diffusion coefficient according to the Randles–Sevcik equation.⁴¹ Moreover, the initial potential during lithium plating on Cu/ZSM-5 was more positive than that on the Cu foil (Figure S10), suggesting a mitigated potential polarization for Li plating.

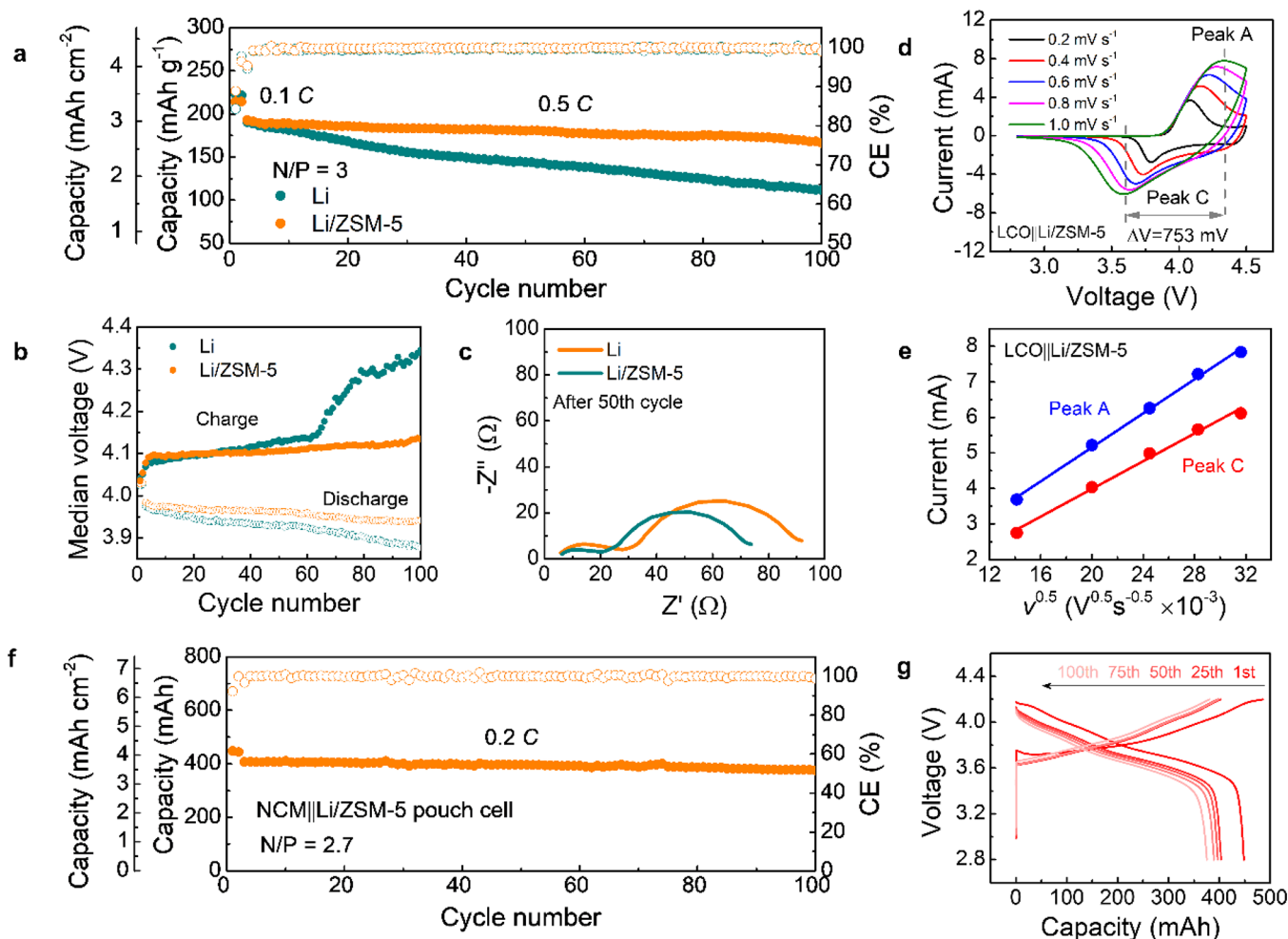


Figure 4. (a) Cycling performances of LCO||Li and LCO||Li/ZSM-5 full cells at an N/P ratio of 3. (b) Charge/discharge median voltage profiles for the LCO||Li and LCO||Li/ZSM-5 full cells at the 100th cycle and (c) the corresponding EIS results after 50 cycles. (d) CV curves of the LCO||Li/ZSM-5 cell at various scan rates ($0.2\text{--}1\text{ mV s}^{-1}$) in the voltage range of 2.8–4.5 V and (e) the corresponding linear fit of the cathodic/anodic peak current as a function of the square root of the scan rates. (f) Cycling performance of the NCM||Li/ZSM-5 pouch cell at 0.2 C and (g) the corresponding voltage–capacity curves of the NCM||Li/ZSM-5 pouch cell at different cycle numbers.

Based on the above results, the Li plating behavior at the Cu/ZSM-5 electrode interface could be explained by the following model (Figure 2k). The continuous consumption of Li^+ leads to a distinct concentration gradient in the space close to the electrode interface for the bare Li electrode. Since the Li^+ concentration gradient in this region is mainly controlled by electromigration and diffusion, this region is referred to as the “diffusion region”. According to the Nernst equation, the decreased Li^+ concentration at the Li anode interface would lead to increased overpotential for lithium plating. The large and nonuniform Li^+ concentration gradient resulted in an uneven distribution of the overpotential for Li^+ reduction within the diffusion region, thus leading to severe concentration polarization. Since the Li metal was preferentially deposited at the area with lower overpotential, the plated Li metal tended to grow in three dimensions in the diffusion region, which easily induced the generation of Li dendrites. On the contrary, due to the improvement of Li^+ transport by the ZSM-5 layer, the Li^+ concentration gradient was minimized, which resulted in reduced overpotential (Figure 2l). The suppression of concentration polarization induced two-dimensional Li metal plating with hindered growth of Li dendrites.

Besides, the rigid interface of the ZSM-5 layer could physically suppress Li dendrite growth.

To investigate the electrochemical Li plating/stripping performance, Li||Li and Li/ZSM-5||Li/ZSM-5 symmetric cells with an electrode thickness of 50 μm (10 mAh cm⁻², Figure S13) were assembled and cycled (Figures S14–S17). As shown in Figure 3a,b, the large and increasing voltage polarization suggested the unstable interface of the bare Li electrode. In contrast, the Li/ZSM-5 electrode displayed a much lower overpotential of 20 mV and a more stable voltage response even after 350 h cycling. The electrochemical performances of symmetric cells under lean electrolyte conditions (20 μL) were also investigated (Figure S18). The Li/ZSM-5||Li/ZSM-5 symmetric cell showed a lower overpotential and longer cycling stability than that of the Li||Li cell. To explore the tuning effect of the ZSM-5 layer, the Li plating behavior of electrodes with the ZSM-5 layer was further investigated. Top-view SEM image of the bare Cu electrode showed a rough surface with dendritic protrusions after initial Li plating under 1 mA cm⁻² and 4 mAh cm⁻² (Figure 3c). The corresponding cross-sectional SEM image revealed the gradual evolution from planar Li to dendritic Li deposits with an increase in the electrochemical deposition time. A loose and whisker-like

deposition layer with a thickness of 29 μm was formed on bare Cu electrode after 4 h Li plating (Figure 3d), displaying a high porosity of 34% (calculated based on the density of metallic lithium). There was no apparent metallic Li on the top surface of the ZSM-5 layer for the Cu/ZSM-5 electrode after 4 h Li plating, which supported the Li plating behavior below the ZSM-5 layer. The Cu/ZSM-5 electrode displayed a dense and uniform Li metal layer with a thickness of ~21 μm under ZSM-5 after Li plating under the same test conditions as the bare Cu electrode, showing a very low porosity of 8% (Figure 3h). The structures of Li/ZSM-5 and Li electrodes after initial Li stripping were compared in Figure S19. An overall uniform surface was shown for the Li/ZSM-5 electrode, while irregular pits with a size of tens of micrometers were observed on the bare Li electrode. The morphology and structure of cycled bare Li and Li/ZSM-5 electrodes were further studied. Much less “dead lithium” (the dark products on the electrode surface) was observed for the Li/ZSM-5 electrode than the bare Li electrode after 50 cycles at 1 mA cm^{-2} and 1 mAh cm^{-2} (Figure S20), which was consistent with the EIS results that the Li/ZSM-5 cell exhibited a lower interfacial resistance than that of the bare Li cell (Figure S21). The surface of cycled bare Li electrode was porous (Figure 3e), and the thickness of the reaction layer reached 30 μm (Figure 3f). Due to the continuous electrolyte consumption and uneven lithium plating, the reaction layer further increased to 80 μm after 100 cycles. Such a thick Li reaction layer with abundant “dead lithium” and accumulated organic byproducts further aggravated the degradation of Li metal anode. Interestingly, the Li/ZSM-5 electrode showed a flat and smooth surface without apparent pores or cracks after 50 cycles (Figure 3i). The thickness of the deposited Li layer was only 10 μm for the 50th cycle, and it slowly increased to 17 μm after 100 cycles (Figure 3j, Figure S22), indicating the much denser Li plating structure than the bare Li electrode.

To further demonstrate the effect of the ZSM-5 interphase in stabilizing the Li metal electrode, the electrochemical performances of Li metal batteries pairing with LiCoO_2 and LiFePO_4 cathodes were investigated (Figures S23–S26). The LCO||Li/ZSM-5 cell with a low N/P ratio of 3 exhibited a high specific capacity of 166 mAh g^{-1} and a high areal capacity of 2.6 mAh cm^{-2} at 0.5 C (1 C = 200 mA g^{-1}) in a wider voltage range from 2.8 to 4.6 V (Figure 4a), delivering a reasonable capacity retention of 83% over 100 cycles. In contrast, the LCO full cell with bare Li showed a fast capacity decay with a decreased capacity retention of 58% (111 mAh g^{-1}) after 100 cycles. The corresponding charge/discharge median voltage profiles of the tested cells are shown in Figure 4b. At the stage of lithium plating, the LCO||Li/ZSM-5 cell performed a stable charge median voltage curve over 100 cycles, while the LCO||Li cell exhibited an obvious voltage rise after 60 cycles. The LCO||Li/ZSM-5 cell also exhibited a higher discharge median voltage than the LCO||Li cell, suggesting the ZSM-5 layer can effectively alleviate the voltage hysteresis (Figure 4b). The corresponding EIS results showed that the LCO||Li/ZSM-5 cell exhibited a charge transfer resistance of 51.5 Ω , which was lower than 63.4 Ω for the LCO||Li cell (Figure 4c). The results of SEM measurements also suggested the more uniform surface structure of the Li/ZSM-5 electrode in comparison to the bare Li electrode after 50 cycles (Figure S27). Figure 4d shows the CV results of the cell with bare Li and Li/ZSM-5 electrodes with different scan rates from 0.2 to 1 mV s^{-1} , and the LCO||Li/ZSM-5 cell showed a smaller voltage separation

than the LCO||Li cell between the redox peaks (peak A and peak C in Figure 4d and Figure S28a, 753 mV for the LCO||Li/ZSM-5 cell and 806 mV for LCO||Li cell). The Li^+ transfer kinetics was further investigated by calculating the diffusion coefficients of Li^+ (D_{Li^+}) based on the Randles-Sevick equation (Figure 4e and Figure S28b). The peak currents of A and C at different scan rates showed linearly proportional relationship to the square root of the voltage scan rates ($\nu^{0.5}$), indicating the diffusion-controlled step of the full cells. Figure S28c shows that the calculated D_{Li^+} values of the LCO||Li/ZSM-5 cell for peaks A and C were $1.38 \times 10^{-6} \text{ cm}^2 \text{ s}^{-1}$ and $8.41 \times 10^{-7} \text{ cm}^2 \text{ s}^{-1}$, respectively, both of which were higher than those of the LCO||Li cell ($1.1 \times 10^{-6} \text{ cm}^2 \text{ s}^{-1}$ for peak A and $6.9 \times 10^{-7} \text{ cm}^2 \text{ s}^{-1}$ for peak C).

Due to the significant role of the ZSM-5 interphase in regulating Li^+ transport and Li plating/stripping behavior, a stable electrochemical performance of the LCO||Li/ZSM-5 full cell was realized even under harsh conditions. With a high areal capacity of over 4 mAh cm^{-2} , small electrolyte dosage of 9 $\mu\text{L mAh}^{-1}$, and low N/P ratio of 2.5, the LCO||Li/ZSM-5 full cell showed much a higher capacity retention of 80% for 70 cycles than the LCO||Li cell at 0.3 C (20% capacity retention for 20 cycles, Figure S29). Furthermore, the potential practical application of the ZSM-5/Li electrode was demonstrated in the pouch cell. Employing a $\text{LiNi}_{0.95}\text{Co}_{0.02}\text{Mn}_{0.03}\text{O}_2$ (NCM) cathode with a high mass loading of 17.3 mg cm^{-2} , areal capacity of 3.7 mAh cm^{-2} , and 50 μm -thick Li anode, the NCM||ZSM-5/Li pouch cell (N/P ratio = 2.7) delivered discharge capacities of 407.7 mAh and 375.7 mAh for the initial and 100th cycle at 0.2 C, respectively (Figure 4f), showing satisfactory cycling performance with a high capacity retention of 92%. Small voltage hysteresis was observed according to the charge–discharge curves of the NCM||Li/ZSM-5 pouch cell (Figure 4g). The excellent cycling performance of the NCM||Li/ZSM-5 pouch cell suggests the huge potential of the Li/ZSM-5 anode for rechargeable Li metal batteries with a high energy density and long cycle life.

In summary, acid–base interaction of PF_6^- and acid sites in the framework of ZSM-5 was designed to stabilize the Li metal anode by employing a readily available zeolite, ZSM-5, as a model system. The improved distribution and mass transfer of Li^+ could facilitate uniform Li plating and suppress concentration polarization at the electrode interface. Benefiting from the multiple effects of a functional ZSM-5 layer, improved electrochemical performance of full cells was realized under high cathode mass loading, low N/P ratio, and small electrolyte dosage. A 400 mAh-level NCM||Li/ZSM-5 pouch cell with a high cathode mass loading of 17.3 mg cm^{-2} and N/P ratio of 2.7 displayed a high capacity retention of 90% for 100 cycles at 0.2 C. The regulation of distribution and mass transfer of Li^+ on the electrode surface by zeolite provides a novel approach for the development of reliable lithium metal electrodes for high energy density Li metal batteries.

■ ASSOCIATED CONTENT

SI Supporting Information

The Supporting Information is available free of charge at <https://pubs.acs.org/doi/10.1021/acs.nanolett.3c00258>.

Details on Li/ZSM-5 fabrication, characterizations, and additional data analyses on the Li^+ transfer regulation (PDF)

AUTHOR INFORMATION

Corresponding Author

Yongming Sun — Wuhan National Laboratory for Optoelectronics (WNLO), Huazhong University of Science & Technology, Wuhan 430074, China;  orcid.org/0000-0001-8528-525X; Email: yongmingsun@hust.edu.cn

Authors

Junmou Du — Wuhan National Laboratory for Optoelectronics (WNLO), Huazhong University of Science & Technology, Wuhan 430074, China

Xiangrui Duan — Wuhan National Laboratory for Optoelectronics (WNLO), Huazhong University of Science & Technology, Wuhan 430074, China

Wenyu Wang — Wuhan National Laboratory for Optoelectronics (WNLO), Huazhong University of Science & Technology, Wuhan 430074, China

Guocheng Li — Wuhan National Laboratory for Optoelectronics (WNLO), Huazhong University of Science & Technology, Wuhan 430074, China

Chunhao Li — Wuhan National Laboratory for Optoelectronics (WNLO), Huazhong University of Science & Technology, Wuhan 430074, China

Yuchen Tan — Wuhan National Laboratory for Optoelectronics (WNLO), Huazhong University of Science & Technology, Wuhan 430074, China

Mintao Wan — Wuhan National Laboratory for Optoelectronics (WNLO), Huazhong University of Science & Technology, Wuhan 430074, China

Zhi Wei Seh — Institute of Materials Research and Engineering, Singapore 138634, Singapore;  orcid.org/0000-0003-0953-567X

Li Wang — Institute of Nuclear & New Energy Technology, Tsinghua University, Beijing 100084, China;  orcid.org/0000-0002-9615-1879

Complete contact information is available at:

<https://pubs.acs.org/10.1021/acs.nanolett.3c00258>

Author Contributions

#J.D. and X.D. contributed equally to this work.

Notes

The authors declare no competing financial interest.

ACKNOWLEDGMENTS

This work was supported by the National Natural Science Foundation of China (Grant Nos. 52272207, 52072137) and the Innovation Fund of Wuhan National Laboratory for Optoelectronics. The authors would like to thank the Analytical and Testing Center of Huazhong University of Science and Technology, Mengheng Wang and Weikun Chen from Xiamen University, as well as the Wuhan National High Magnetic Field Center for providing the facilities to conduct the characterizations. Z.W.S. acknowledges the Agency for Science, Technology and Research (Central Research Fund Award).

REFERENCES

- (1) Dunn, B.; Kamath, H.; Tarascon, J.-M. Electrical energy storage for the grid: A battery of choices. *Science* **2011**, *334*, 928–935.
- (2) Miao, Y.; Hynan, P.; von Jouanne, A.; Yokochi, A. Current Li-Ion battery technologies in electric vehicles and opportunities for advancements. *Energy* **2019**, *12* (6), 1074.
- (3) Tian, Y.; Zeng, G.; Rutt, A.; Shi, T.; Kim, H.; Wang, J.; Koettgen, J.; Sun, Y.; Ouyang, B.; Chen, T.; Lun, Z.; Rong, Z.; Persson, K.; Ceder, G. Promises and challenges of next-generation "beyond Lithium" batteries for electric vehicles and grid decarbonization. *Chem. Rev.* **2021**, *121* (3), 1623–1669.
- (4) Lin, D.; Liu, Y.; Cui, Y. Reviving the lithium metal anode for high-energy batteries. *Nat. Nanotechnol.* **2017**, *12* (3), 194–206.
- (5) Liu, J.; Bao, Z.; Cui, Y.; Dufek, E. J.; Goodenough, J. B.; Khalifah, P.; Li, Q.; Liaw, B.; Liu, P.; Manthiram, A.; Meng, Y. S.; Subramanian, V. R.; Toney, M. F.; Viswanathan, V.; Whittingham, M. S.; Xiao, J.; Xu, W.; Yang, J.; Yang, X.; Zhang, J. Pathways for practical high-energy long-cycling lithium metal batteries. *Nat. Energy* **2019**, *4* (3), 180–186.
- (6) Xu, W.; Wang, J.; Ding, F.; Chen, X.; Nasybulin, E.; Zhang, Y.; Zhang, J. Lithium metal anodes for rechargeable batteries. *Energy Environ. Sci.* **2014**, *7* (2), 513–537.
- (7) Cheng, X.; Zhang, R.; Zhao, C.; Zhang, Q. Toward safe lithium metal anode in rechargeable batteries: A review. *Chem. Rev.* **2017**, *117* (15), 10403–10473.
- (8) Duan, J.; Zheng, Y.; Luo, W.; Wu, W.; Wang, T.; Xie, Y.; Li, S.; Li, J.; Huang, Y. Is graphite lithiophobic or lithiophilic? *Natl. Sci. Rev.* **2020**, *7* (7), 1208–1217.
- (9) Chen, S.; Dai, F.; Cai, M. Opportunities and challenges of high-energy lithium metal batteries for electric vehicle applications. *ACS Energy Lett.* **2020**, *5* (10), 3140–3151.
- (10) Guo, Y.; Li, H.; Zhai, T. Reviving lithium-metal anodes for next-generation high-energy batteries. *Adv. Mater.* **2017**, *29* (29), 1700007.
- (11) Wang, Q.; Liu, B.; Shen, Y.; Wu, J.; Zhao, Z.; Zhong, C.; Hu, W. Confronting the challenges in lithium anodes for lithium metal batteries. *Adv. Sci.* **2021**, *8* (17), No. e2101111.
- (12) Albertus, P.; Babinec, S.; Litzelman, S.; Newman, A. Status and challenges in enabling the lithium metal electrode for high-energy and low-cost rechargeable batteries. *Nat. Energy* **2018**, *3* (1), 16–21.
- (13) Zheng, X.; Huang, L.; Ye, X.; Zhang, J.; Min, F.; Luo, W.; Huang, Y. Critical effects of electrolyte recipes for Li and Na metal batteries. *Chem.* **2021**, *7* (9), 2312–2346.
- (14) Jiang, Z.; Jin, L.; Han, Z.; Hu, W.; Zeng, Z.; Sun, Y.; Xie, J. Facile generation of polymer-alloy hybrid layers for dendrite-free lithium-metal anodes with improved moisture stability. *Angew. Chem., Int. Ed. Engl.* **2019**, *58* (33), 11374–11378.
- (15) Pathak, R.; Chen, K.; Gurung, A.; Reza, K. M.; Bahrami, B.; Pokharel, J.; Baniya, A.; He, W.; Wu, F.; Zhou, Y.; Xu, K.; Qiao, Q. Fluorinated hybrid solid-electrolyte-interphase for dendrite-free lithium deposition. *Nat. Commun.* **2020**, *11* (1), 93.
- (16) Ye, H.; Zheng, Z. J.; Yao, H. R.; Liu, S. C.; Zuo, T. T.; Wu, X. W.; Yin, Y. X.; Li, N. W.; Gu, J. J.; Cao, F. F.; Guo, Y. G. Guiding uniform Li plating/stripping through lithium-aluminum alloying medium for long-life Li metal batteries. *Angew. Chem., Int. Ed. Engl.* **2019**, *58* (4), 1094–1099.
- (17) Tang, W.; Yin, X.; Kang, S.; Chen, Z.; Tian, B.; Teo, S. L.; Wang, X.; Chi, X.; Loh, K.; Lee, H.; Zheng, G. W. Lithium silicide surface enrichment: A solution to lithium metal battery. *Adv. Mater.* **2018**, *30* (34), 1801745.
- (18) Zhang, Z.; Jin, Y.; Zhao, Y.; Xu, J.; Sun, B.; Liu, K.; Lu, H.; Lv, N.; Dang, Z.; Wu, H. Homogenous lithium plating/stripping regulation by a massproducible Zn particles modified Li-metal composite anode. *Nano Res.* **2021**, *14*, 3999–4005.
- (19) Zhao, J.; Liao, L.; Shi, F.; Lei, T.; Chen, G.; Pei, A.; Sun, J.; Yan, K.; Zhou, G.; Xie, J.; Liu, C.; Li, Y.; Liang, Z.; Bao, Z.; Cui, Y. Surface fluorination of reactive battery anode materials for enhanced stability. *J. Am. Chem. Soc.* **2017**, *139* (33), 11550–11558.
- (20) Fu, L.; Wang, X.; Wang, L.; Wan, M.; Li, Y.; Cai, Z.; Tan, Y.; Li, G.; Zhan, R.; Seh, Z.; Sun, Y. A salt-in-metal anode: Stabilizing the solid electrolyte interphase to enable prolonged battery cycling. *Adv. Funct. Mater.* **2021**, *31* (19), 2010602.
- (21) Liu, X.; Liu, J.; Qian, T.; Chen, H.; Yan, C. Novel organophosphate-derived dual-layered interface enabling air-stable

- and dendrite-free lithium metal anode. *Adv. Mater.* **2020**, *32* (2), 1902724.
- (22) Chen, H.; Pei, A.; Lin, D.; Xie, J.; Yang, A.; Xu, J.; Lin, K.; Wang, J.; Wang, H.; Shi, F.; Boyle, D.; Cui, Y. Uniform high ionic conducting lithium sulfide protection layer for stable lithium metal anode. *Adv. Energy Mater.* **2019**, *9* (22), 1900858.
- (23) Lee, Y.; Ma, B.; Bai, P. Concentration polarization and metal dendrite initiation in isolated electrolyte microchannels. *Energy Environ. Sci.* **2020**, *13* (10), 3504–3513.
- (24) Tang, C.; Dillon, S. In situ scanning electron microscopy characterization of the mechanism for Li dendrite growth. *J. Electrochem. Soc.* **2016**, *163* (8), A1660–A1665.
- (25) Ju, Z.; Xie, Q.; Sheng, O.; Wu, X.; Tan, Y.; Hong, M.; Tao, X.; Liang, Z. Biomass-derived anion-anchoring nano-CaCO₃ coating for regulating ion transport on Li metal surface. *Nano Lett.* **2022**, *22*, 5473–5480.
- (26) Yan, Y.; Shu, C.; Zheng, R.; Li, M.; Ran, Z.; He, M.; Hu, A.; Zeng, T.; Xu, H.; Zeng, Y. Modulating Sand's time by ion-transport enhancement toward dendrite-free lithium metal anode. *Nano Res.* **2022**, *15* (4), 3150–3160.
- (27) Brissot, C.; Rosso, M.; Chazalviel, J.-N.; Lascaud, S. Dendritic growth mechanisms in lithium-polymer cells. *J. Power Sources* **1999**, 81–82, 925–929.
- (28) Xu, Y.; Gao, L.; Shen, L.; Liu, Q.; Zhu, Y.; Liu, Q.; Li, L.; Kong, X.; Lu, Y.; Wu, H. Ion-transport-rectifying layer enables Li-metal batteries with high energy density. *Matter* **2020**, *3* (5), 1685–1700.
- (29) Li, X.; Tian, Y.; Shen, L.; Qu, Z.; Ma, T.; Sun, F.; Liu, X.; Zhang, C.; Shen, J.; Li, X.; Gao, L.; Xiao, S.; Liu, T.; Liu, Y.; Lu, Y. Electrolyte interphase built from anionic covalent organic frameworks for lithium dendrite suppression. *Adv. Funct. Mater.* **2021**, *31*, 2009718.
- (30) Wu, H.; Lou, X. Metal-organic frameworks and their derived materials for electrochemical energy storage and conversion: Promises and challenges. *Sci. Adv.* **2017**, *3*, eaap9252.
- (31) Mehek, R.; Iqbal, N.; Noor, T.; Amjad, M. Z. B.; Ali, G.; Vignarooban, K.; Khan, M. A. Metal-organic framework based electrode materials for lithium-ion batteries: A review. *RSC Adv.* **2021**, *11* (47), 29247–29266.
- (32) Rahimi, N.; Karimzadeh, R. Catalytic cracking of hydrocarbons over modified ZSM-5 zeolites to produce light olefins: A review. *Appl. Catal. A-Gen.* **2011**, *398* (1–2), 1–17.
- (33) Pfaffenhuber, C.; Gobel, M.; Popovic, J.; Maier, J. Soggy-sand electrolytes: status and perspectives. *Phys. Chem. Chem. Phys.* **2013**, *15* (42), 18318–35.
- (34) Pfaffenhuber, C.; Hoffmann, F.; Fröba, M.; Popovic, J.; Maier, J. Soggy-sand effects in liquid composite electrolytes with mesoporous materials as fillers. *J. Mater. Chem. A* **2013**, *1* (40), 12560–12567.
- (35) Bhattacharyya, A. J. Ion transport in liquid salt solutions with oxide dispersions: "Soggy sand" electrolytes. *J. Phys. Chem. Lett.* **2012**, *3* (6), 744–50.
- (36) Lawson, S.; Baamran, K.; Newport, K.; Rezaei, F.; Rownaghi, A. Screening of adsorbent/catalyst composite monoliths for carbon capture-utilization and ethylene production. *ACS Appl. Mater. Interfaces* **2021**, *13* (46), 55198–55207.
- (37) Xiao, H.; Zhang, J.; Wang, X.; Zhang, Q.; Xie, H.; Han, Y.; Tan, Y. A highly efficient Ga/ZSM-5 catalyst prepared by formic acid impregnation and in situ treatment for propane aromatization. *Catal. Sci. Technol.* **2015**, *5* (8), 4081–4090.
- (38) Zhou, H.; Zhang, F.; Ji, K.; Gao, J.; Liu, P.; Zhang, K.; Wu, S. Relationship between acidity and activity on propane conversion over metal-modified HZSM-5 catalysts. *Catalysts* **2021**, *11*, 1138.
- (39) Qiao, B.; Leverick, G. M.; Zhao, W.; Flood, A. H.; Johnson, J. A.; Shao-Horn, Y. Supramolecular regulation of anions enhances conductivity and transference number of lithium in liquid electrolytes. *J. Am. Chem. Soc.* **2018**, *140* (35), 10932–10936.
- (40) Wahyudi, W.; Ladelta, V.; Tsatsaris, L.; Alsabban, M.; Guo, X.; Yengel, E.; Faber, H.; Adilbekova, B.; Seitkhan, A.; Emwas, A. H.; Hedhili, M.; Li, L. J.; Tung, V.; Hadjichristidis, N.; Anthopoulos, T.; Ming, J. Lithium-ion desolvation induced by nitrate additives reveals new insights into high performance lithium batteries. *Adv. Funct. Mater.* **2021**, *31* (23), 2101593.
- (41) Shen, L.; Wu, H.; Liu, F.; Shen, J.; Mo, R.; Chen, G.; Tan, G.; Chen, J.; Kong, X.; Lu, X.; Peng, Y.; Zhu, J.; Wang, G.; Lu, Y. Particulate anion sorbents as electrolyte additives for lithium batteries. *Adv. Funct. Mater.* **2020**, *30* (49), 2003055.

Recommended by ACS

Reversible, Dendrite-Free, High-Capacity Aluminum Metal Anode Enabled by Aluminophilic Interface Layer

Yahan Meng, Wei Chen, *et al.*

MARCH 06, 2023
NANO LETTERS

READ ▶

Incorporating α -Al₂O₃ Nanodots into Expanded Graphite Anodes toward Stable Fast Charging for Lithium-Ion Batteries

Huirong Ma, Zhiyong Mao, *et al.*

FEBRUARY 01, 2023
ACS APPLIED ENERGY MATERIALS

READ ▶

Reversible Al Metal Anodes Enabled by Amorphization for Aqueous Aluminum Batteries

Chunshuang Yan, Guihua Yu, *et al.*

JUNE 18, 2022
JOURNAL OF THE AMERICAN CHEMICAL SOCIETY

READ ▶

Rational Design of an Artificial SEI: Alloy/Solid Electrolyte Hybrid Layer for a Highly Reversible Na and K Metal Anode

Dongjun Li, Yan Yu, *et al.*

OCTOBER 12, 2022
ACS NANO

READ ▶

Get More Suggestions >